Journal of Applied Polymer Science

Enhancement of Pervaporation Performance of Composite Membranes Through *In Situ* Generation of Silver Nanoparticles in Poly(vinyl alcohol) Matrix

H.G. Premakshi, Ashok M. Sajjan, Arjumand A. Kittur, Mahadevappa Y. Kariduraganavar
Department of Chemistry, Karnatak University, Dharwad 580 003, Karnataka, India
Correspondence to: M. Y. Kariduraganavar (E-mail: mahadevappak@yahoo.com)

ABSTRACT: Composite membranes were prepared from an aqueous solution of poly(vinyl alcohol) (PVA) and silver sulphate. The silver nanoparticles were generated *in situ* before crosslinking PVA matrix by reduction of silver ions using sodium borohydride. Physico-chemical properties of the resulting composite membranes were studied using Fourier transform infrared spectroscopy (FTIR), UV–vis spectroscopy (UV–vis), thermogravimetric analysis (TGA), Wide-angle X-ray diffraction (WAXD), scanning electron microscopy (SEM), and universal testing machine (UTM). The UV–vis spectrum shows a single peak at 410 nm due to surface plasmon absorption of silver nanoparticles. This surely specified that silver nanoparticles are generated in PVA matrix. The membranes were under go pervaporation (PV) for separation of water from isopropanol at different temperatures. The results indicated that hydrophilicity and amorphous nature of the membranes were increased with increasing silver nanoparticles in PVA matrix. The swelling and separation performance of the membranes were studied. Both permeation flux and separation factor were increased with increasing silver nanoparticles in PVA matrix. The results showed that the membrane containing 2.5 mass% of Ag salt exhibited excellent PV performance. The values of total flux and flux of water are almost closed to each other, indicating that membranes could be effectively used to break the azeotropic point of water-isopropanol. The long-term test was performed at room temperature and ascertained that membranes were durable up to 30 days for the dehydration of IPA. On the basis of the estimate Arrhenius activation energy values, the efficiency of the membranes was discussed. The calculated ΔH_s values are negative for all the membranes, indicating that Longmuir's mode of sorption is predominant. © 2014 Wiley Periodicals, Inc. J. Appl. Polym. Sci. **2015**, *132*, 41248.

KEYWORDS: composites; crosslinking; membranes; swelling; thermogravimetric analysis

Received 13 December 2013; accepted 30 June 2014
DOI: 10.1002/app.41248

INTRODUCTION

Metal nanoparticles incorporated polymer matrices have attracted tremendous research interest in both academia and industry due to their structural diversity, flexibility, and tenability as well as high porosity.[1] Such materials have a wide range of applications, viz., gas storage and separation, selective heterogeneous catalysis, carbon dioxide capture, and guest dependent luminescence, etc.[1–5] Among the metal nanoparticles, silver nanoparticles signify as promising functional fillers due to their unique characters and find enormous applications in various fields such as intercalation of materials for electrical batteries and optical receptors,[6,7] polarizing filters, catalysis in chemical reactions, bio-labeling, sensors, bio-active materials,[8–10] signal enhancers in surface-enhanced Raman scattering (SERS) based enzyme immuno assay and antimicrobial agents.[11,12]

The incorporation of silver nanoparticles influences on the properties of polymers, is intensively investigated recently, since introduction of even a small amount of nanoparticles into the polymeric matrix can greatly change the mechanical, optical, and other properties of a material.[13] Silver nanoparticles have stronger electron transmission absorption bands (surface plasmons) in the visible range than other metals.[14] These investigations suggest that the introduction of nanosized particles into polymer matrix alters its properties.

PV is a well accepted membrane separation process for the separation of azeotropic and close boiling liquids because of its simple operation and energy saving efficiency as compared to all other conventional distillation processes.[15,16] However, the technical feasibility of this process largely depends on the membrane and its properties. Generally, most of the developed membranes exhibit a trade-off phenomenon between flux and selectivity. As a result, PV becomes incompetent process for a large scale separation. To circumvent this problem, considerable efforts have been adopted by suitably modifying the membranes. Among them are: incorporation of selective zeolites into

membrane matrix,[17,18] development of hybrid membranes,[19,20] incorporation of ZIF-8 material,[21] introduction of silane compounds as crosslinking agents,[22–24] etc. For instance, Kittur et al.[17] and Kariduraganavar et al.,[25] respectively studied the pervaporation (PV) separation of zeolite and TiO_2 filled membranes for the separation of water-isopropanol systems. Similarly, Uragami et al.,[20] Liu et al.,[22] and Zhang et al.[26] developed silica based organic–inorganic hybrid membranes. All these membranes demonstrated exceptionally high permeability and good selectivity by overcoming the trade-off phenomenon. This is because, inorganic fillers as well as metals in polymer matrix offer consistent and unique opportunities to obtain the specific transport properties. Recently, it is very well demonstrated that nanoparticles provide preferential pathways for the permeation and have resulted to novel hydrophilic membranes for the efficient PV separation of organic-water mixtures.[21] Among the hydrophilic membrane materials, poly(vinyl alcohol) (PVA) is a widely studied material for the dehydration of organic mixtures owing to its good chemical stability, film forming ability, and high hydrophilicity.[27,28] The greater swelling nature of PVA membranes in an aqueous solution results to an increase of both solubility and diffusivity, and accordingly lowers the water permselectivity.[29] To improve its stability and permeation properties, we have synthesized silver nanoparticles and incorporated them appropriately in PVA matrix so as to increase its PV performance. Generally, there are two methods which have been employed for the incorporation of metal nanoparticles into a polymer matrix.[30] In the first method, the colloidal metal nanoparticles are prepared separately by reducing the metal salt using an appropriate reducing agent and dispersed in polymer matrix with agitation (*ex situ*). However, the generated nanoparticles are stabilized by using appropriate capping agents. Otherwise, the developed metal nanoparticles slowly undergo agglomeration. To avoid this, the second method (*in situ*) is generally employed more frequently, wherein the generated metal nanoparticles are stabilized by the polymer itself, and thereby the addition of capping agents is to be avoided completely. In view of this, *in situ* method is more convenient and serves as a stabilizer, control the size of the nanoparticles and attain the uniform distribution.[31]

Therefore, current investigation focuses on the preparation of silver nanoparticles by *in situ* method in PVA solution. The content of silver nanoparticles was varied so as to improve the overall performance of the resulting membranes. Before casting the polymer solution, it was subjected to crosslinking with a known amount of glutaraldehyde to minimize the swelling property of the membrane. The physico–chemical properties of the resulting membranes were studied using different techniques such as UV-visible, FTIR, WAXD, TGA, SEM, and UTM. These membranes were successfully employed for PV separation of water-isopropanol mixtures. The values of permeation flux, separation selectivity and diffusion coefficients were evaluated. The results were discussed in term of PV separation efficiency of the membranes.

EXPERIMENTAL

Materials

PVA ($\bar{M}_w \sim 125{,}000$), glutaraldehyde, isopropanol, silver sulfate, and sodium borohydride ($NaBH_4$) were purchased from S.D. fine Chemicals, Mumbai, India. All other solvents and reagents were of analytical grade and used without further purification. Double distilled water was used throughout the study.

Membrane Preparation

PVA (4 g) was dissolved in 80 mL of deareated distilled water with constant stirring for about 24 h at room temperature. The solution was filtered using a fritted glass disc-filter to remove the undissolved residue particles. It was then subjected to sonication at a fixed frequency of 38 kHz (Grant XB6, UK) for 30 min so as to break the possible aggregated molecules. To this, 1 mL of glutaraldehyde (25%) was added at 80°C for *in situ* crosslinking and stirred for 1 h at the same temperature. Further to remove the air bubbles the solution was left overnight. The resulting clear solution was cast onto a glass plate with the aid of a casting knife in a dust-free atmosphere. After being dried in air for about 48 h, the membrane was peeled-off and later annealed at 60°C for 24 h in an inert atmosphere and was designated as M.

To prepare nanocomposite hybrid membrane, a known amount of silver sulfate was added into a PVA solution. In each time the amount of PVA was kept constant. The mixed solution was stirred for about 1 h and then 10 mg of sodium borohydride was added. To break the aggregated silver particles and to improve their dispersion in the polymer matrix, the resulting clear yellow-sol was stirred for about 24 h and subjected to sonication for about 30 min at a fixed frequency of 38 kHz (Grant XB6, UK). The resulting solution was poured onto a clean glass plate and the membrane was dried as aforementioned. The Ag particles dispersed in PVA via *in situ* of nanocolloids and they underwent reduction from Ag^+ to Ag atoms in presence of $NaBH_4$. The amount of silver with respect to PVA was varied as 1, 1.5, 2, and 2.5 mass% and the membranes thus obtained were designated as M-1, M-2, M-3, and M-4, respectively. The scheme for the preparation of Ag-PVA nanocomposite hybrid membranes is illustrated in Figure 1. The thickness of these membranes was measured at different points using a peacock dial thickness gauge (Model G, Ozaki MFG., Japan) with an accuracy of ± 2 μm and the average thickness was considered for calculation. The thickness of the membranes was found to be 40 ± 2 μm.

UV–Visible Absorbance Spectroscopy

Absorbance spectra of crosslinked PVA and its composite membrane samples were recorded using UV–visible absorbance spectroscopy (UV–visible absorbance spectrophotometer 15–210). The spectra were recorded in the range of 300–800 nm.

Fourier Transform Infrared (FTIR) Spectroscopy

The interaction between Ag-Nps and the PVA matrix was studied using FTIR spectroscopy (Nicolet, Impact-410, USA). The spectra were recorded in the range of 400–4000 cm^{-1} under a hydraulic pressure of 400 kg/cm^2. In each scan, the amount of membrane sample and KBr were kept constant in order to estimate the changes in the intensities of the characteristic peaks with respect to the amount of silver.

Wide-Angle X-ray Diffraction (WAXD)

Wide-angle X-ray diffraction measurements of crosslinked PVA and its composite membranes were carried out with a Brucker's

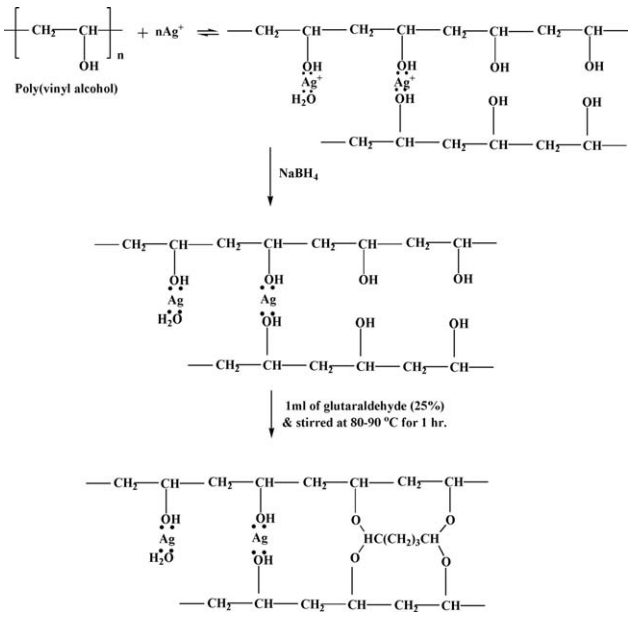

Figure 1. Scheme for the synthesis of composite membranes.

D-8 advanced wide-angle X-ray diffraction at room temperature using Ni-filtered Cu Kα source. The diffraction was operated in the range of 5°–50° at 40 kV and 30 mA with a scanning speed of 8°/min at an angle 2θ.

Thermogravimetric Analysis (TGA)

Thermograms of the crosslinked PVA and its composite membranes were recorded using a thermogravimetric analyzer (DSC Q 20, TA Instruments, Waters LLC, USA) at a heating rate of 10°C/min under nitrogen atmosphere. The weight of the membrane samples taken for each record was about 6–9 mg.

Scanning Electron Microscopy (SEM)

The surface and cross-section views of the crosslinked PVA and its composite membrane were recorded using scanning electron microscope (JEOL, JSM-400 Å, Tokyo, Japan). Before taking the photographs, all the specimens were coated with a conductive layer (400 Å) of sputtered gold.

Mechanical Properties

The mechanical properties such as tensile strength and percent elongation at break of the crosslinked PVA and its composite membranes were measured at 25°C using Hounsfield H25KS Universal Testing Machine (UTM), UK with a speed of 50 mm/min. The gauge dimension of the test sample was 25 × 50 mm. For each sample, three specimens were tested and results were averaged.

Swelling Measurements

The dried membrane samples were weighed and immersed in different compositions of water-isopropanol mixtures at 30°C for 24 h to attain equilibrium swelling. The swollen membrane samples were taken out at regular intervals, wiped carefully with tissue paper to remove the surface adhered solvent and weighed as quickly as possible. The same procedure was repeated at least for three times and, the results were averaged. The percent degree of swelling (DS) was calculated as follows:

$$DS(\%) = \left(\frac{W_s - W_d}{W_d}\right) \times 100 \quad (1)$$

where W is the mass of the membrane. Subscripts s and d refer to the swollen and dry membrane, respectively.

Long-Term Durability Test

To assess the durability of the membranes, the crosslinked PVA and its composite membranes were subjected to long-term test by immersing in an 85 wt % of aqueous isopropanol at room temperature for 48 days in different air-tight bottles. For every 4 days, membranes were removed from the solution and weighed immediately after careful blotting with a tissue paper. The same membranes were subjected to deswelling and weighed. The procedure was repeated till the membranes start losing their weights.

Pervaporation Experiments

PV experiments were carried out using the in-house designed set up as reported in our previous articles.[32,33] The capacity of the feed chamber was about 250 cm^3 and the effective membrane surface area in contact with the feed mixture was 34.23 cm^2. The vacuum in the downstream side of the apparatus was maintained [1.333224 × 10^3 Pa (10 Torr)] with a two-stage vacuum pump (Toshniwal, Chennai, India). The composition of water in the feed mixture was varied from 5 to 25 mass%. Before performing PV experiments, the test membrane was allowed to reach equilibrium for about 2 h in the feed compartment with a known volume of feed mixture. After a steady state was attained, the permeate was collected in a trap immersed in liquid nitrogen jar on the downstream side at a regular intervals of time. The experiments were carried out at 30, 40, and 50°C. The flux was calculated by weighing the permeate on a digital microbalance. The composition of water and isopropanol in the permeate was calculated by measuring the refractive index of the permeate using an Abbe's refractometer (sensitivity ± 0.0001, Atago-3T, Japan), and by comparing it with a standard plot that was previously established with the known compositions of water-isopropanol mixtures. All the experiments were performed at least three times, and the average results were reported. The results of permeation for water-isopropanol mixtures during the PV were reproducible within the range of ±5%.

On the basis of the PV data, separation performance of the membranes was evaluated in terms of total flux (J) and separation selectivity (α_{sep}). These were calculated respectively using the following equations:

$$J = \frac{W}{A.t} \quad (2)$$

$$\alpha_{sep} = \frac{P_w / P_{IPA}}{F_w / F_{IPA}} \quad (3)$$

where W is the mass of permeate (kg); A is the membrane area (m^2); t is the permeation time (h); P_w and P_{IPA} are the respective mass fraction of water and isopropanol in the permeate; F_w and F_{IPA} are the mass fraction of water and isopropanol in the feed, respectively.

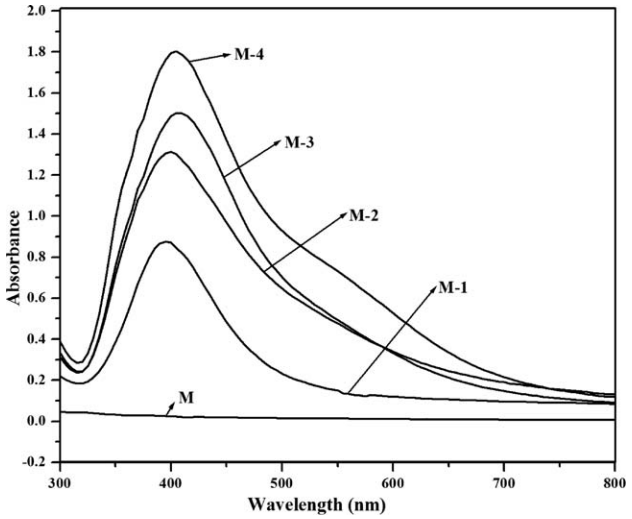

Figure 2. UV–visible absorption spectra of crosslinked PVA and its Ag-Nps incorporated composite membranes: (M) 0 mass%; (M-1) 1 mass%; (M-2) 1.5 mass%; (M-3) 2 mass%; (M-4) 2.5 mass% of Ag-Nps.

RESULTS AND DISCUSSION

Membrane Characterization

UV–Visible Analysis. The absorption spectra of crosslinked PVA and its composite membranes are shown in Figure 2. It is observed that no absorbance peak was found in the investigated wavelength range for the crosslinked PVA membrane (M). However, all the composite membranes showed a broad peak and whose maximum absorbance occurred at 410 nm. This is attributed to an occurrence of surface plasmon resonance of silver nanoparticles (Ag-Nps) in the resulting composite membranes.[34] As the content of silver nanoparticles was increased in the membranes, the absorbance at 410 nm was increased. This ensures the formation of Ag-Nps as well as their increased concentration in the membrane matrix. This is very well demonstrated in the actual photographs of the crosslinked PVA and its Ag-Nps incorporated composite membrane films presented in Figure 3.

FTIR Analysis. The spectra of crosslinked PVA and its composite membranes were recorded using FTIR and the spectra thus obtained are presented in Figure 4. The crosslinked PVA (M) exhibits a characteristic band at around 3400 cm^{-1} and multiple bands between 1000 and 1150 cm^{-1}, which correspond to —OH and C—O stretching vibrations, respectively. Upon

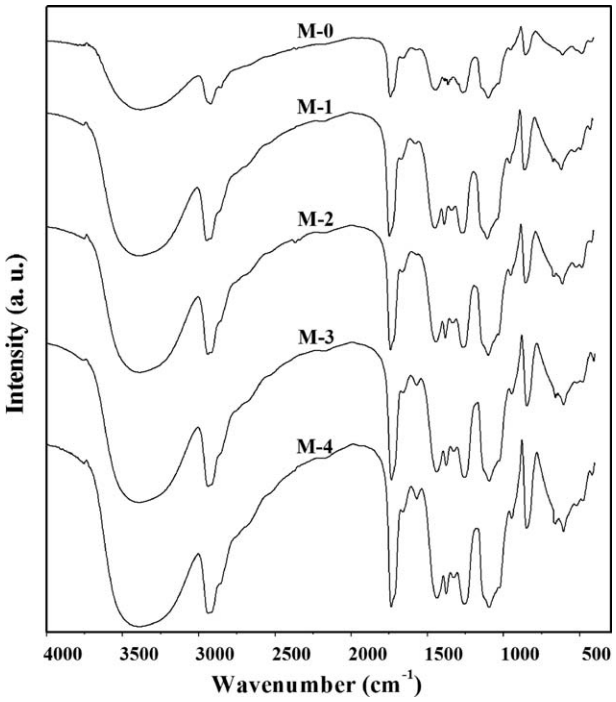

Figure 4. FTIR spectra of crosslinked PVA and its Ag-Nps incorporated composite membranes: (M) 0 mass%; (M-1) 1 mass%; (M-2) 1.5 mass%; (M-3) 2 mass%; (M-4) 2.5 mass% of Ag-Nps.

developing the Ag-Nps in the crosslinked PVA matrix, the intensity of —OH band was significantly increased from membrane M to M-1. This is due to an establishment of interaction between Ag-Nps and -OH groups of PVA. The intensity of this band was correspondingly increased from membrane M-1 to M-4 as the content of Ag-Nps increased in the PVA matrix. This is expected due to increased hydrophilic character in the membrane owing to the presence of silver nanoparticles, which are known to exhibit hydrophilic behavior.[35] A new band is also observed at 660 cm^{-1} in the composite membranes and its intensity was increased marginally with increasing the Ag-Nps. This ensures the formation of hydrogen bonds in the PVA matrix.[36] On the basis of these evidences, it is concluded that Ag-Nps enhance the rigidity of the crosslinked PVA membrane owing to an establishment of both hydrogen bonding and interaction of —OH groups with the Ag-Nps, which would play an important role in enhancing the both flux and selectivity of the resulting membranes.

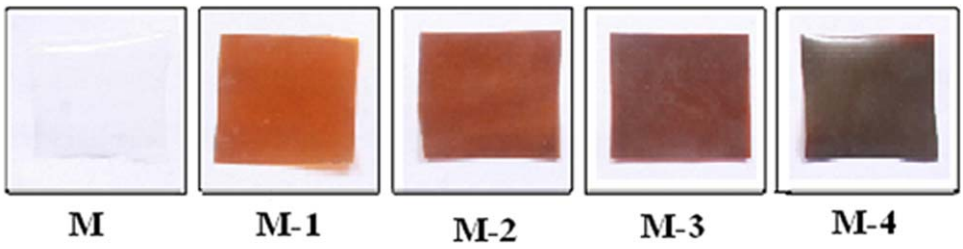

Figure 3. Photographs of the crosslinked PVA and its Ag-Nps incorporated composite membranes. [Color figure can be viewed in the online issue, which is available at wileyonlinelibrary.com.]

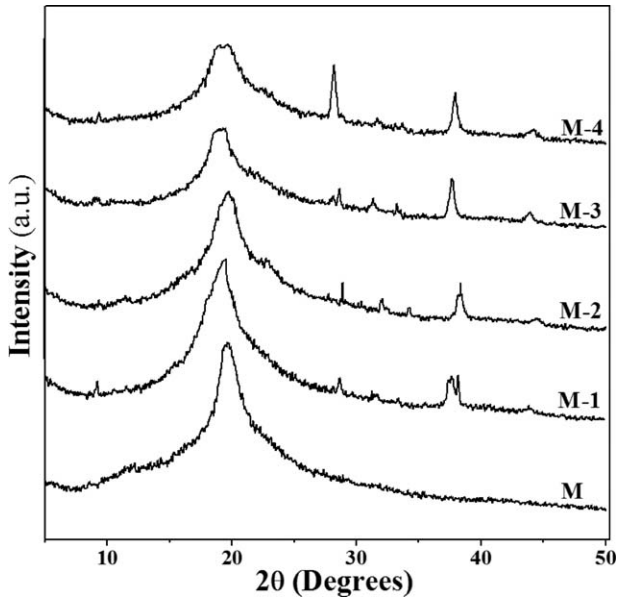

Figure 5. Wide-angle X-ray diffraction patterns of crosslinked PVA and its Ag-Nps incorporated composite membranes: (M) 0 mass%; (M-1) 1 mass%; (M-2) 1.5 mass%; (M-3) 2 mass%; (M-4) 2.5 mass% of Ag-Nps.

Wide-Angle X-ray Diffraction Analysis (WAXD). Degree of crystallinity of the crosslinked PVA and its composite membranes was studied by WAXD and the resulting diffraction profiles are given in Figure 5. The diffraction pattern of crosslinked PVA shows a typical peak at around $2\theta = 20°$, indicating that the crosslinked PVA contains both crystalline and amorphous domains in the matrix.[37] However, the intensity of this typical peak was correspondingly decreased with increasing the Ag-Nps (M-1 to M-4). This is due to an establishment of hydrogen bonding and interaction of —OH groups with the Ag-Nps. This effect is predominant as the content of Ag-Nps was increased in the membranes. This has led to an increase of amorphous region, which generally favors the diffusion of permeants through the membrane and thereby enhances the selective permeants in the composite membranes.

Thermogravimetric Analysis (TGA). Thermal stability of the crosslinked PVA and its composite membranes was analyzed using TGA under nitrogen atmosphere, and the resulting thermograms are shown in Figure 6. All the membranes exhibited three consecutive steps for weight loss and the first weight loss is around 5%, which occurred between 60 and 110°C. This is attributed to desorption of physically absorbed water molecules in the membrane. Although second weight loss was started at around 230°C for all the membranes, the percentage weight loss was about 60% varied from 230 to 380°C, which corresponds to the decomposition of PVA chain. This weight loss was decreased correspondingly with increasing the amount of Ag-Nps in crosslinked PVA matrix. The third weight loss occurred between 380 and 480°C, and is attributed to decomposition of glutaraldehyde. All these clearly suggest that Ag-Nps incorporated membranes demonstrated better thermal stability than that of crosslinked PVA membrane.

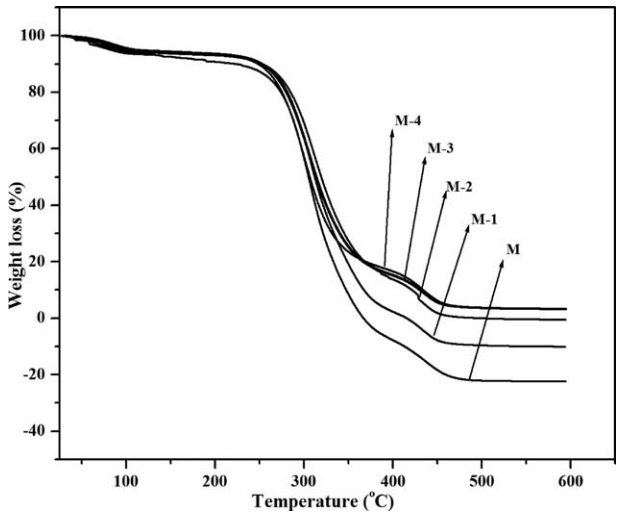

Figure 6. Thermogravimetric analysis of crosslinked PVA and its Ag-Nps incorporated composite membranes: (M) 0 mass%; (M-1) 1 mass%; (M-2) 1.5 mass%; (M-3) 2 mass%; (M-4) 2.5 mass% of Ag-Nps.

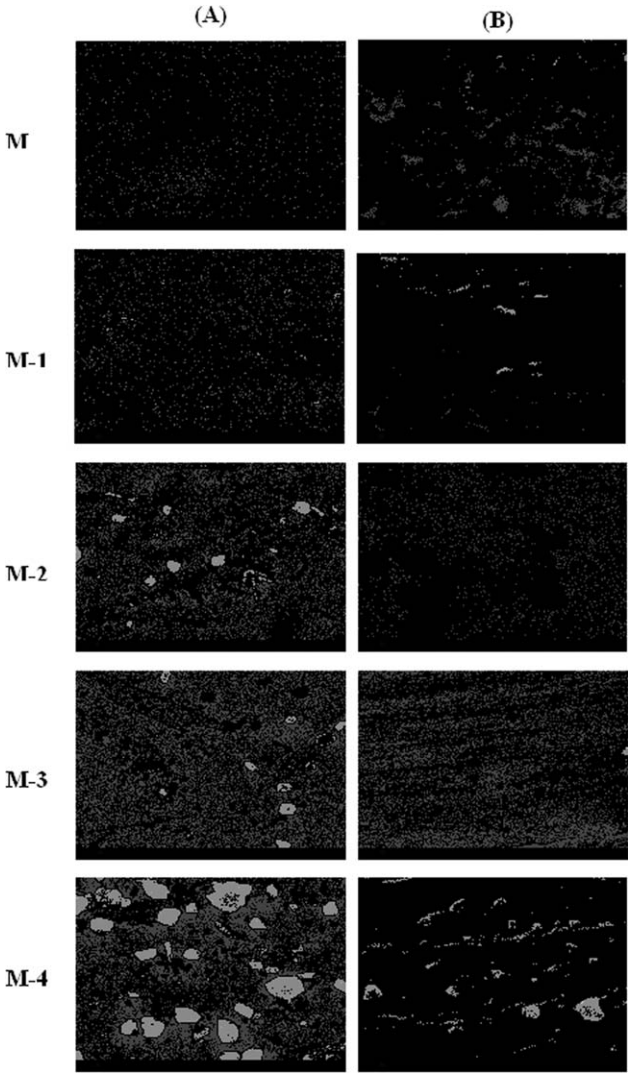

Figure 7. SEM micrographs of crosslinked PVA and its Ag-Nps incorporated composite membranes: (A) surface view and (B) cross-sectional view.

Table I. Tensile Property of Crosslinked PVA and its Ag-Nps Incorporated Composite Membranes

Membrane	Tensile strength (MPa)	Elongation at break (%)
M	76	86
M-1	63	56
M-2	54	50
M-3	51	36
M-4	47	25

Scanning Electron Microscopy (SEM) Analysis. Figure 7 illustrates the SEM photographs of the surface and cross-sectional views of crosslinked PVA and its composite membranes. At lower concentration, Ag-Nps were distributed evenly throughout the crosslinked PVA matrix. However, at higher concentration, we can notice Ag-Nps on the surface as well as in the bulk of the material. Further the photographs explicitly show that silver particles implanted in the membrane matrix have no voids around them. This ensures that Ag-Nps incorporated membranes obtained here are free from the possible defects and can be employed for PV process without any difficulty.

Mechanical Properties

Tensile strength and percent elongation of a membrane often tell its suitability for PV applications. The effect of Ag-Nps on the tensile strength and percent elongation of the crosslinked membranes were studied and the data thus obtained are summarized in Table I. It could be seen from the data that both tensile strength and percent elongation were respectively decreased from 76 to 47 MPa and 86 to 25% with increasing the content of Ag-Nps. This was expected due to an establishment of ionic clusters in the membranes and this becomes prominent as the content of Ag-Nps was increased in the membrane. Despite of the fact, the resulting membranes are suitable for the PV separation.

Effects of Feed Composition and Ag-Nps on Membrane Swelling

The degree of membrane swelling played an important role in dehydration of organics that controls the transport of permeating molecules under the chemical potential gradient. Figure 8 represents the effects of feed composition and Ag-Nps on the membrane swelling at 30°C. It is observed that the DS was increased almost linearly for all the membranes with increasing the mass% of water in the feed. This appears a strong interaction occurring between water molecules and the intractable groups such as —OH and Ag-Nps present in the membrane. However, DS was also increased systematically with increasing the Ag-Nps in the membrane and the same trend is remained throughout the investigated water composition. This arise an enhancement of hydrophilic character in the membrane owing to the presence of Ag-Nps. This was very well demonstrated in the FTIR study.

Effect of Ag-Nps on Long-Term Durability of the Membrane

From Figure 9, it is clearly observed that the DS is almost constant for all the composite membranes up to 30 days and

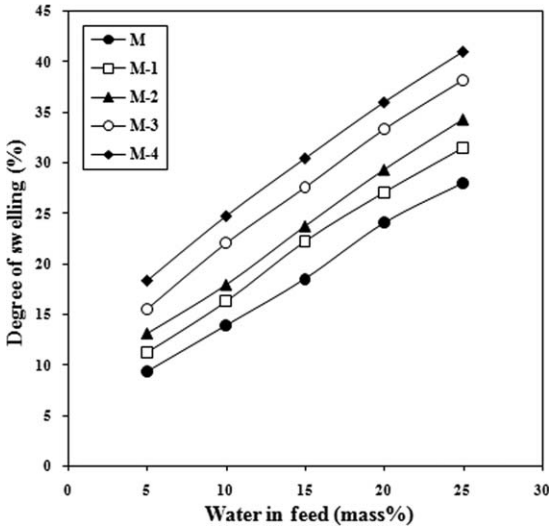

Figure 8. Variation of degree of swelling with different mass% of water in the feed for crosslinked PVA and its Ag-Nps incorporated composite membranes.

beyond this, the DS was gradually decreased. This suggests that composite membranes developed with Ag-Nps are durable up to 30 days for the dehydration of IPA. This is due to increased hydrophilicity of the membranes due to the incorporation of Ag-Nps. This is very well demonstrated in the FTIR study. The *in situ* generation of Ag-Nps in the polymer matrix always serves as the stabilizer. On the other hand, the crosslinked PVA membrane is durable only up to 18 days and beyond this, it was started loosing its mass% gradually. The same behavior is observed in deswelling data, which are included in the Figure 9. Further, it is noticed that the decreasing tendency in swelling beyond 30 days is prominent for the membranes having higher loading of Ag-Nps. This is expected due to a greater leaching effect observed in higher loading of Ag-Nps. The degree of deswelling also decreases with increasing the Ag-Nps in the

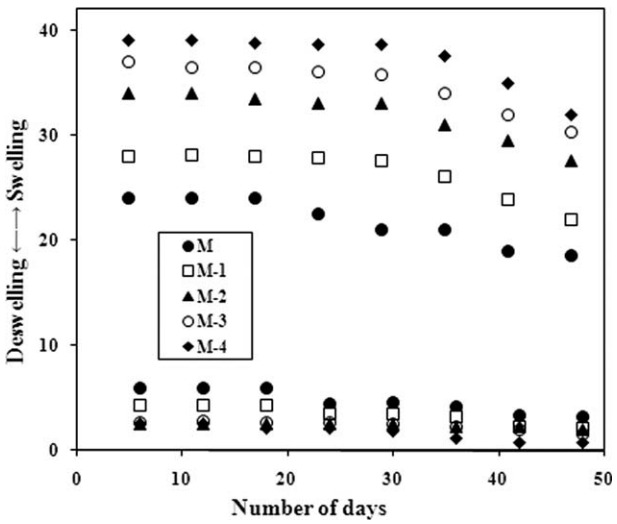

Figure 9. Variation of swelling and deswelling as a function of time for crosslinked PVA and its Ag-Nps incorporated composite membranes at 85 mass% of IPA in the feed.

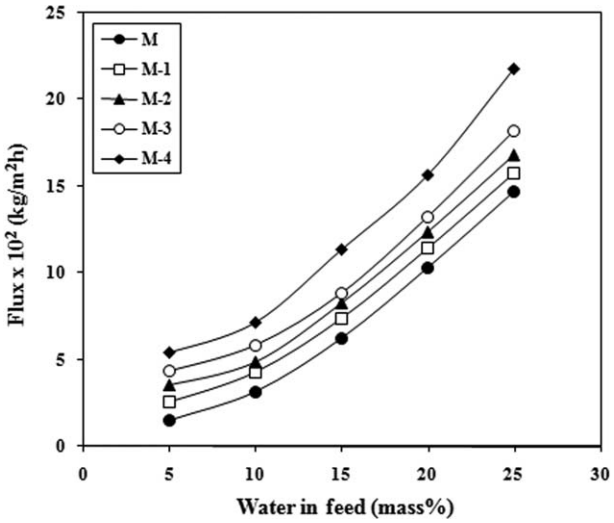

Figure 10. Variation of total pervaporation flux with different mass% of water in the feed for crosslinked PVA and its Ag-Nps incorporated composite membranes.

crosslinked membrane. On the basis of these, it is ascertained that Ag-Nps improve the long-term stability of the membrane for PV dehydration of IPA.

Effects of Feed Composition and Ag-Nps on Pervaporation

Figure 10 shows the effects of feed composition and Ag-Nps on the total permeation flux for all the membranes at 30°C. It is found that the total permeation flux was increased almost linearly for all the membranes with increasing the mass% of water in the feed and this is almost in accordance with the swelling study. This is because of increased selective interactions between water molecules and the membrane and obviously, the interaction is predominant at higher concentration of water in the feed. Similarly, the total permeation flux was increased with increasing Ag-Nps in the membrane. This is because of increased hydrophilicity as discussed in the swelling study. This is expected owing to an establishment of greater interaction between Ag-Nps and water molecules. Second, the increased

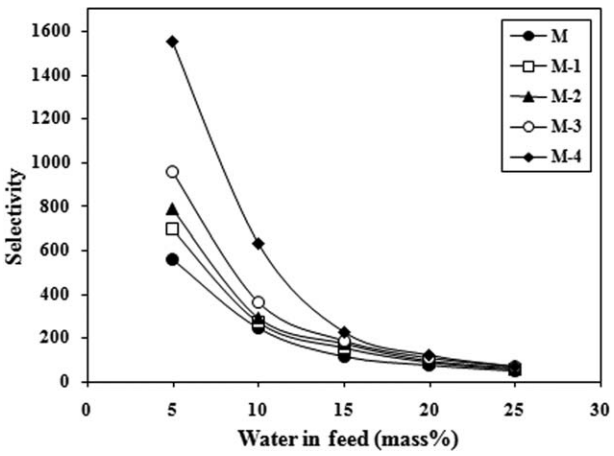

Figure 11. Variation of separation selectivity with different mass% of water in the feed for crosslinked PVA and its Ag-Nps incorporated composite membranes.

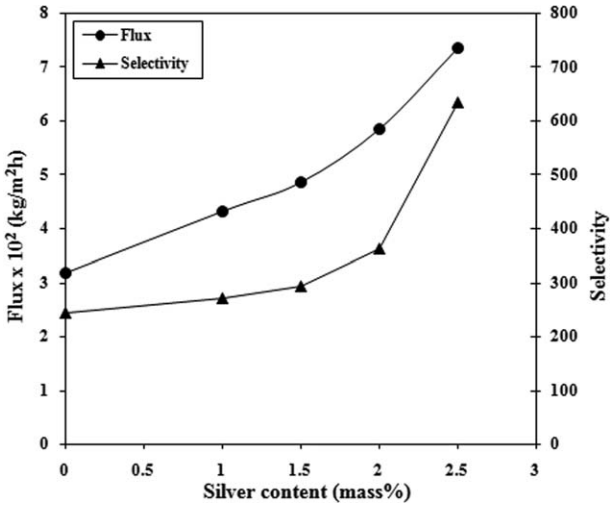

Figure 12. Variation of flux and selectivity with different mass% of Ag-Nps at 10 mass% of water in the feed.

amorphous character of the membrane by the incorporation of Ag-Nps as evidenced from WAXD analysis is also responsible for the increase of flux. These two are reasonably contributing for the overall increase of permeation flux with increasing the Ag-Nps in the crosslinked PVA membrane.

The selectivity of a membrane in PV is based on interaction between membrane and the permeating molecules, and the molecular size of the permeating species. Figure 11 displays the effects of water compositions and Ag-Nps on the selectivity of all the membranes. It is noticed that there was a remarkable decrease in the selectivity for all the membranes with increasing the water composition from 5 to 15 mass%. On the other hand, this was decreased gradually with further increasing the water composition in the feed. At higher concentration of water in the feed, the membrane swells greatly and thereby upstream surface of the membrane becomes plasticized owing to an establishment of a strong interaction between the membrane and water molecules. The resulting

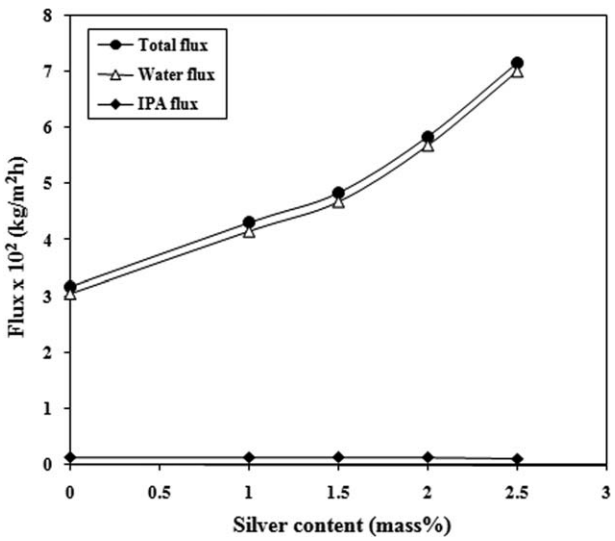

Figure 13. Variation of total flux, fluxes of water, and isopropanol with different mass% of Ag-Nps at 10 mass% of water in the feed.

Table II. Diffusion Coefficients of Water and Isopropanol for All Membranes at Different Mass% of Water in the Feed

Mass% of water	$D_w \times 10^8$ (cm^2/s)					$D_{IPA} \times 10^{10}$ (cm^2/s)				
	M	M-1	M-2	M-3	M-4	M	M-1	M-2	M-3	M-4
5	5.97	7.82	8.04	9.62	12.20	5.97	5.81	5.58	5.45	4.61
10	6.20	8.47	9.55	11.63	14.41	10.73	10.42	10.10	8.52	7.43
15	8.06	9.68	10.80	11.91	15.21	22.90	20.91	20.51	19.30	18.70
20	9.94	11.20	12.11	13.01	15.52	43.70	41.80	41.71	39.31	38.14
25	12.12	12.52	13.12	14.22	17.22	78.12	72.72	69.82	69.20	68.54

plasticized upstream membrane surface allows some of isopropanol molecules along with selective permeants, which causes a negative impact on the membrane's selectivity.

On the contrary, the selectivity was increased remarkably from membrane M-1 to M-4, upon increasing the Ag-Nps in the membrane. This was assigned to increased selective interaction between membrane and the water molecules owing to the presence of Ag-Nps in the crosslinked matrix. This was further reveals from the Figure 12, in which flux and selectivity were plotted as a function of silver content in the membranes at 10 mass% of water in the feed. Because of crosslinking or incorporation of fillers into the membrane matrix packing density of the membranes increases, as a result the permeation flux decreases and selectivity increases.[18,37] However, in the present study both permeation flux and selectivity were increased with increasing Ag-NPs in the membrane. This is due to a trade-off phenomenon existing between flux and selectivity in PV process, a significant enhancement of hydrophilicity and establishment of greater interaction by the incorporation of Ag-Nps in the crosslinked PVA matrix overcome this phenomenon.

The efficiency of membranes was assessed by plotting the individual fluxes as a function of mass% of silver at 10 mass% of water in the feed are shown in Figure 13. It is clearly indicated that the total flux and flux of water are almost closed to each other, whereas the flux of isopropanol is negligibly small, indicating that the membranes developed in the present study by the incorporation of Ag-Nps are highly selective towards water with a wonderful improvement in the flux as compared to membrane M. On the basis of this plot, it is further concluded that membrane containing 2.5 mass% of Ag-Nps demonstrated excellent flux and selectivity among the membranes developed in the present study.

Diffusion Coefficient

A proper understanding of the PV, the solution-diffusion mechanism is accepted by several researchers. According to this mechanism, PV process consists of three consecutive steps: sorption of the permeant from the feed mixture to the membrane, diffusion of the permeant in the membrane and desorption of the permeant to the vapor phase on the downstream side of the membrane.[38] Thus, rate of permeation and selectivity are governed by the solubility and diffusivity of each component of the feed liquid to be separated. In the PV process, the diffusion step controls the transport of penetrants, because of the establishment of fast equilibrium distribution between bulk feed and the upstream surface of a membrane.[39] It is therefore, to understand the mechanism of transport of molecules important to estimate the diffusion coefficient, D_i of penetrating molecules.

From Fick's law of diffusion, the diffusion coefficient can be expressed as:[40]

$$J_i = -D_i \frac{dC_i}{dx} \tag{4}$$

where J is the permeation flux per unit area (kg/m^{2}s); D is the diffusion coefficient (m^2/s); C is the concentration of permeant in the membrane (kg/m^3); subscript i stands for water or isopropanol; and x is the diffusion length (m). For simplicity it is assumed that the concentration profile along the diffusion length is linear and thus, diffusion coefficient D_i can be calculated with the following modified equation:[41,42]

$$D_i = \frac{J_i \delta}{C_i} \tag{5}$$

where δ is the membrane thickness. The calculated values of D_i at 30°C are presented in Table II. It is observed that the diffusion coefficient of water was increased from M to M-4 while systematically decreasing the diffusion coefficient of IPA.

On the contrary, the diffusion coefficients of both water and IPA were increased with increasing the water concentration in the feed. However, compare to isopropanol, the magnitude of

Table III. Pervaporation Flux and Separation Selectivity of All Different Membranes at Different Temperatures for 10 Mass% of Water in the Feed

Temp. (°C)	$J \times 10^2$ (kg/m^{2}h)					α_{sep}				
	M	M-1	M-2	M-3	M-4	M	M-1	M-2	M-3	M-4
30	3.18	4.31	4.84	5.85	7.16	244	271	293	361	634
40	6.25	6.82	7.08	8.24	10.19	197	213	271	293	329
50	10.30	10.87	12.92	13.23	14.19	144	152	184	213	244

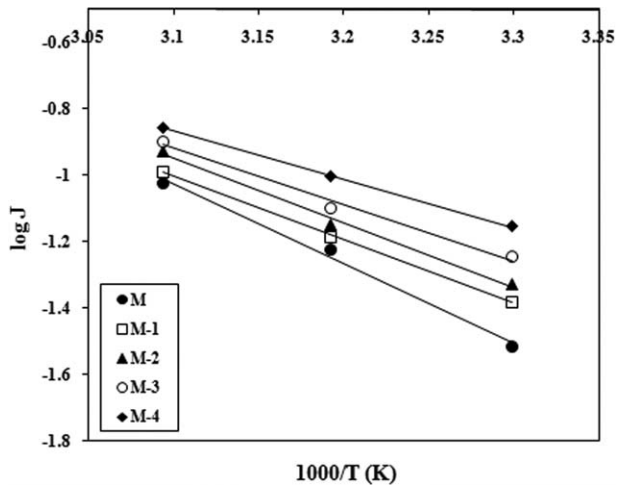

Figure 14. Variation of log J with temperature for crosslinked PVA and its Ag-Nps incorporated composite membranes at 10 mass% of water in the feed.

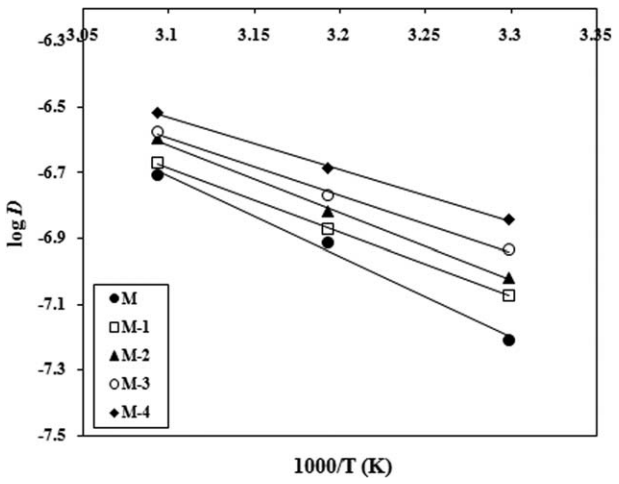

Figure 15. Variation of log D with temperature for crosslinked PVA and its Ag-Nps incorporated composite membranes at 10 mass% of water in the feed.

diffusion coefficients of water was quite high, suggesting that the membranes developed in the present study are highly selective towards water. This is very well explained in Figure 13.

Effect of Temperature on Membrane Performance

The effect of operating temperature on PV performance was studied for all the membranes at 10 mass% of water in the feed, and values thus obtained are presented in Table III. It is noticed that with increasing temperature the permeation rate was increased for all the membranes while decreasing the separation selectivity. This may be because of two reasons. First, as the temperature increases the vapor pressure difference also increases between the upstream and downstream side of the membranes and this in turn improvement in the transport of driving force. Second, an increase of temperature promotes the thermal motion of polymer chain segments, creating more free-volume in the polymer matrix. However, the latter reason is ruled out in the present study since the experiments were performed well below the glass transition temperature of the crosslinked PVA.[43] Therefore, the driving force played a major role in transporting the associated molecules along with the selective permeants. This results to an increase of total permeation flux while decreasing the selectivity. Thus, the temperature dependence of permeation and diffusion has prompted us to estimate the activation energies for permeation and diffusion using the Arrhenius type equation[44]:

$$X = X_o \exp\left(\frac{-E_x}{RT}\right) \quad (6)$$

where X represents permeation (J) or diffusion (D). X_o is a constant representing pre-exponential factor of J_o or D_o. E_x denotes the activation energy for permeation or diffusion depending upon the transport process under consideration, and R is a gas constant T is a temperature (K). As the feed temperature increases, the vapor pressure in the feed compartment also increases, but the vapor pressure at the permeate side is not affected. This leads to an increase of driving force with increasing the temperature.

Arrhenius plots of log J and log D versus temperature are shown in Figures 14 and 15, respectively. In both the cases, a linear trend was observed, suggesting that permeability and diffusivity follow an Arrhenius trend. From the least-squares fits of these linear plots, we have estimated the activation energies for total permeation (E_p) and total diffusion (E_D). Similarly, the activation energies for permeation of water (E_{pw}) and isopropanol (E_{pIPA}), and diffusion of water (E_{Dw}) were estimated, but the plots are not given to minimize the figures. However, the values thus obtained are presented in Table IV.

From Table IV, it is observed that the apparent activation energy values for water permeation (E_{pw}) are almost two times lower than those of isopropanol permeation (E_{pIPA}), suggesting that membranes developed here have higher separation efficiency towards water. The activation energy values for water permeation (E_{pw}) and total permeation (E_p) are almost close to each other, signifying that coupled-transport of both water and isopropanol is minimal as due to higher selective nature of the membranes. It is further noticed that as the Ag-Nps were increased in membrane M-1 to M-4, the activation energy values of both E_p and E_D were systematically decreased. This is due to increased hydrophilicity with increasing the content of Ag-Nps in the membrane matrix, and obviously the energy required for transport of selective permeants was reduced.

Table IV. Arrhenius Activation Parameters for Permeation and Diffusion and Heat of Sorption

Parameters (kJ/mol)	M	M-1	M-2	M-3	M-4
Ep	47.92	39.85	37.64	33.19	27.87
ED	48.13	40.81	37.91	33.81	28.14
Epw	46.93	39.14	36.63	32.51	26.97
EpIPA	68.32	60.14	58.018	53.95	52.40
EDw	47.87	40.23	37.49	33.51	27.94
ΔHs	−0.21	−0.96	−0.27	−0.62	−0.27

The estimated E_p and E_D values ranged between 47.92 and 27.87, and 48.13 and 28.14 kJ/mol, respectively. Using these values, we have further calculated the heat of sorption as:

$$\Delta H_s = E_p - E_D. \quad (7)$$

The resulting ΔH_s values are presented in Table IV. So we can observe the hole filling mechanism by negative values of ΔH_s sorption.[45] This infers that, Langmuir's mode of sorption is predominant indicating an exothermic contribution.

CONCLUSIONS

In the present study, composite membranes were prepared using crosslinked PVA and silver nanoparticles. The membranes were subjected to separate water-isopropanol mixtures at three different temperatures. An increase of Ag-Nps results to a simultaneous increase of both permeation flux and selectivity. This was discussed on the basis of enhancement of hydrophilic character and increased rigidity due to greater interaction. From the experimental data, the total flux and water flux are closed each other for all the membranes, conclude that the prepared membranes are highly selective towards water. Among the membranes studied, the membrane containing 2.5 mass% of Ag-Nps demonstrated the highest separation selectivity of 634 with a flux of 7.16×10^{-2} kg/m^{2}h. The permeation flux was increased and selectivity decreased with increase in temperature, it has been found that decreased interaction between permeants and the membrane. The composite membranes containing the highest amount of Ag-Nps showed seriously lower activation energy values. This was explained based on increased hydrophilicity and greater interaction. The membranes exhibit lower activation energy values for water permeation (E_{pw}) than that of isopropanol permeation (E_{pIPA}), manifesting that the membranes developed here have demonstrated excellent separation efficiency towards water. So we can observe the hole filling mechanism by negative values of ΔH_s sorption, and involving Langmuir's mode of sorption.

ACKNOWLEDGMENTS

The authors thank the Department of Physics, Indian Institute of Science, Bangalore.

REFERENCES

1. Jeffrey, R.; Long, J.; Yaghi, O. *Chem. Soc. Rev.* **2009**, *38*, 1213.
2. Férey, G. *Chem. Soc. Rev.* **2008**, *37*, 191.
3. Liu, B. *J. Mater. Chem.* **2012**, *22*, 10094.
4. Heilmann, A. Springer Series in Material Science; Springer: Berlin, **2002**.
5. Ramesh, G. V.; Porel, S.; Radhakrishnan, T. P. *Chem. Soc. Rev.* **2009**, *38*, 2646.
6. Joerger, R.; Klaus-Joerger, T.; Olsson, E.; Granqvist, C. G. *Solar Energy* **2000**, *69*, 27.
7. Schultz, S.; Smith, D. R.; Mock, J. J.; Schultz, D. A. *Proc. Natl. Acad. Sci. U S A* **2000**, *97*, 996.
8. Handley, D. A.; Hayat, M. A. Colloidal Gold: Principles, Methods and Applications; Ed. Academic Press: San Diego, CA, **1989**; Vol. *1*, p. 1.
9. Dubas, S. T.; Pimpan, V. *Talanta* **2008**, *76*, 29.
10. Blaker, J. J.; Nazhat, S. N.; Boccaccini, A. R. *Biomaterials* **2004**, *25*, 1319.
11. Chen, J.; Lo, Y.; Liang, Y.; Jiang, J.; Shen, G.; Yu, R. *Anal. Sci.* **2009**, *25*, 347.
12. Morones, J. R.; Elechiguerra, J. L.; Camacho, A.; Holt, K.; Kouri, J. B.; Ramirez, J. T.; Yacama, J. M. *Nanotechnology* **2005**, *16*, 2346.
13. Goddard, W. A.; Brenner, D. W.; Lyshevski, S. E.; Lafrate, G. J. Handbook of Nanoscience Engineering, and Technology; CRC press: London, UK, **2003**.
14. Kutsenko, A. S.; Granchak, V. M. *Theor. Exp. Chem.* **2009**, *45*, 313.
15. Semenova, S. I.; Ohya, H.; Soontarapa, K. *Anal Rev Desalin.* **1997**, *110*, 251.
16. Urtiaga, A. M.; Gorri, E. D.; Casado, C.; Ortiz, I. *Sep. Purif. Tech.* **2003**, *32*, 207.
17. Kittur, A. A.; Kulkarni, S. S.; Aralaguppi, M. I.; Kariduraganavar, M. Y. *J. Membr. Sci.* **2005**, *247*, 75.
18. Kariduraganavar, M. Y.; Kittur, A. A.; Kulkarni, S. S.; Ramesh, K. *J. Membr. Sci.* **2004**, *238*, 165.
19. Liu, Y. L.; Su, Y. H.; Lee, K. R.; Lai, J. Y. *J. Membr. Sci.* **2005**, *25*, 1233.
20. Uragami, T.; Katayama, T.; Miyata, T.; Tamura, H.; Shiraiwa, T.; Higuchi, A. *Biomacromolecules* **2004**, *51*, 567.
21. Liu, X. L.; Li, Y. S.; Zhu, G. Q.; Ban, Y. J.; Xu, L.Y.; Yang, W. S. *Angew. Chem. Int. Ed.* **2011**, *50*, 10636.
22. Liu, Y. L.; Hsu, C. Y.; Su, Y. H.; Lai, J. Y. *Biomacromolecules* **2005**, *6*, 368.
23. Kulkarni, S. S.; Kittur, A. A.; Aralaguppi, M. I.; Kariduraganavar, M. Y. *J. Appl. Polym. Sci.* **2004**, *94*, 1304.
24. Kariduraganavar, M. Y.; Kulkarni, S. S.; Kittur, A. A. *J. Membr. Sci.* **2005**, *246*, 83.
25. Kariduraganavar, M. Y.; Varghese, J. G.; Choudhari, S. K.; Olley, R. H. *Ind. Eng. Chem. Res.* **2009**, *48*, 4002.
26. Zhang, Q. G.; Liu, Q. L.; Chen, Y.; Chen, J. H. *Ind. Eng. Chem. Res.* **2007**, *46*, 913.
27. Will, B. *J. Membr. Sci.* **1992**, *68*, 119.
28. Alghezawi, N.; Sanli, O.; Aras, L.; Asman, G. *Chem. Eng. Process.* **2005**, *44*, 51.
29. Srinivasa Rao, P.; Smitha, B.; Sridhar, S.; Krishnaiah, A. *Sep. Purif. Technol.* **2005**, *44*, 244.
30. Gautam, A.; Ram, S. *Mater. Chem. Phys.* **2010**, *119*, 266.
31. Calinescu, I.; Patrascu, M.; Gavrila, A. I.; Trifan, A.; Boscornea, C. U. P. B. *Sci. Bull. Series B*, **2011**, *73*, 4.
32. Sajjan, A. M.; Jeevan Kumar, B. K.; Kittur, A. A.; Kariduraganavar, M. Y. *J. Membr. Sci.* **2013**, *425*, 77.
33. Rachipudi, P. S.; Kittur, A. A.; Sajjan, A. M.; Kariduraganavar, M. Y. *J. Membr. Sci.* **2013**, *441*, 83.
34. Gautam, A.; Ram, S. *Phys. Solid State A* **2009**, *206*, 1471.

35. Vasiliev, A. N.; Gulliver, E. A.; Khinast, J. G.; Riman, R. E. *Surf. Coats Technol.* **2009**, *203*, 2841.

36. González-Campos, J. B.; Prokhorov, E.; Sanchez, I. C.; Luna-Bárcenas, J. G.; Manzano-Ramirez, A.; González-Hernández, J.; opez-Castro, Y. L.; del Rio, R. E. *J. Nanomater.* **2012**, *2012*, 11.

37. Sajjan, A. M.; Kariduraganavar, M. Y. *J. Membr. Sci.* **2013**, *438*, 8.

38. Kulkarni, S. S.; Tambe, S. M.; Kittur, A. A.; Kariduraganavar, M. Y. *J. Membr. Sci.* **2006**, *285*, 420.

39. Huang, R. Y. M.; Yeom, C. K. *J. Membr. Sci.* **1991**, *58*, 33.

40. Hwang, S. T.; Kammermeyer, K. Membrane in Separations; Wiley Interscience: New York, **1975**.

41. Yamasaki, A.; Iwatsubo, T.; Masuoka, T.; Mizoguchi, K. *J. Membr. Sci.* **1994**, *89*, 111.

42. Kusumochayo, S. P.; Sudoh, M. *J. Membr. Sci.* **1999**, *161*, 77.

43. Rachipudi, P. S.; Kariduraganavar, M. Y.; Kittur A. A.; Sajjan, A. M. *J. Membr. Sci.* **2011**, *383*, 224.

44. Kittur, A. A.; Kariduraganavar, M. Y.; Toti, U. S.; Ramesh, K.; Aminabhavi, T. M. *J. Appl. Polym. Sci.* **2003**, *90*, 2441.

45. Weinkauf, D. H.; Paul, D. R.; Koros, W. J. Ed. ASC Symp. Ser. Am. Chem. Soc. Washington, DC, **1990**, *423*, 61.